Phase-Field Theory of Ion Intercalation Kinetics

Martin Z. Bazant*
Departments of Chemical Engineering and Mathematics,
Massachusetts Institute of Technology, Cambridge, Massachusetts 02139, USA

CONSPECTUS

Interest in electrochemistry is surging, driven by new applications in energy conversion, water treatment, materials processing, and biotechnology. As geometries shrink to the nanoscale, the rate-limiting step is often ion intercalation (i.e. reversible insertion) into a host solid for transport or storage. For example, oxygen intercalates into a ceramic electrolytes in solid oxide fuel cells, and lithium intercalates into carbon or metal oxide nanoparticles in Li-ion batteries. The standard phenomenological model for electrode kinetics is the Butler-Volmer equation, which fits the current-voltage relation in many situations and can be justified (in certain limits) by the Marcus theory of charge transfer. Existing theories, however, provide little guidance as to the form of the exchange-current prefactor to account for configurational entropy, elastic stress, phase transformations, and other non-idealities arising in ion intercalation.

These challenges are exemplified by the high-rate cathode material, Li_xFePO_4 (LFP), which has a strong tendency to phase separate into Li-rich and Li-poor phases that is believed to limit its performance. Phase separation was originally thought to occur as an isotropic "shrinking core" in each particle, but experiments later revealed striped phase boundaries along the active facet. Meanwhile, dramatic rate enhancement was attained with LFP nanoparticles, and classical battery models could not predict the role of phase separation. This Account describes the development of a theory that answers this question via a variational formulation of Faradaic reaction kinetics for ionic solids and concentrated solutions.

The theory is based on non-equilibrium thermodynamics, consistent with Cahn-Hilliard phase-field models for the solid host. Butler-Volmer and Marcus kinetics are reformulated for concentrated solutions using activity coefficients. The theory is applied to lithium insertion in transition metal oxides. For phase-separating solids, such as LFP, the intercalation rate is enhanced by concentration gradients and elastic coherency strain. This causes exposed phase boundaries to propagate as "intercalation waves" at low current. Above a small critical current, homogeneous reactions are favored, which helps to explain the high rate capability of LFP nanoparticles. The theory also predicts similar phenomena in porous electrodes with phase-separating nanoparticles. Narrow reaction fronts with mosaic instabilities at low currents become broadened and limited by electrolyte diffusion at high currents.

I. INTRODUCTION

The standard model of electrode kinetics is the Butler-Volmer (BV) equation[1, 2],

$$I = I_0 \left(e^{-\alpha_c n e \eta / k_B T} - e^{\alpha_a n e \eta / k_B T} \right) \tag{1}$$

which relates the total current I due to the Faradaic reaction, $O + ne^- \rightarrow R$, which converts the oxidized state O to the reduced state R and consumes n electrons, to the exchange current I_0 and overpotential $\eta = \Delta\phi - \Delta\phi^{eq}$, where $\Delta\phi$ is the interfacial voltage whose Nernst equilibrium value is $\Delta\phi^{eq}$. For a simple single-step charge-transfer reaction, the anodic and cathodic charge-transfer coefficients α_a and α_c should satisfy $\alpha_a = 1 - \alpha$ and $\alpha_c = \alpha$ with a symmetry factor, $0 < \alpha < 1$, although the same form is often fitted to more complicated experimental voltage dependence. The microscopic theory of charge transfer [3], pioneered by R. A. Marcus and honored by the Nobel Prize in Chemistry [4], provides justification for the BV equation and a means to estimate its parameters in dilute solutions [1].

Since ion intercalation occurs concentrated solid solutions, the reaction rate is affected by packing entropy, elastic strain, and other non-idealities, which are neglected in classical theories. In Li-ion battery simulations [2, 5–7], only excluded volume has been considered, by empirically modifying the exchange current

$$I_0(c) = k(c_{max} - c)^{\alpha_c} c^{\alpha_a} \tag{2}$$

where c_{max} is the maximum lithium concentration in the solid. Moreover, the Nernst potential $\Delta\phi^{eq}(c)$ is fitted to the open circuit voltage, and the chemical diffusivity $D^{chem}(c)$ in the solid is adjusted to fit discharge curves. In a thermodynamically consistent theory, however, these properties must all derive from the local lithium activity at the nanoscale.

Advances in Li-ion batteries increasingly rely on the unusual kinetics of nanoparticles, as best illustrated by lithium iron phosphate, Li_xFePO_4 (LFP). In the seminal LFP paper, Padhi et al. [8] concluded that "the material is very good for low-power applications" but "at higher

*Electronic address: bazant@mit.edu

current densities there is a reversible decrease in capacity that... is associated with the movement of a two-phase interface" (between Li-rich and Li-poor phases). Over the next decade, LFP ironically became a popular high-power material [9–11], but only in nanoparticle form. Understanding the role of phase separation in this reversal of fortune turned out to be a major scientific challenge.

It is now understood that phase separation is strongly suppressed in LFP nanoparticles, to some extent in equilibrium [12–14], but especially under applied current [14–17], since reaction limitation [18], anisotropic lithium transport [19, 20], elastic coherency strain [14, 21–23], and surface energy [15, 24, 25] are enhanced. At low currents, however, anisotropic nucleation and growth can also occur in nanoparticles [14, 15, 18, 26], leading to stochastic multi-particle intercalation [27–30]. These phenomena could not be described by traditional battery models [2, 5], which assume a spherical "shrinking core" phase boundary [6, 7].

This Account summarizes my struggle to develop a theory of intercalation kinetics in phase-separating electrodes [13–15, 18, 23, 30–35] by combining charge-transfer theory [3] with concepts from statistical physics [36, 37] and non-equilibrium thermodynamics [38, 39]. The work began when my postdoc, G. Singh, found the paper of Chen et al. [40] revealing striped phase boundaries in LFP, looking nothing like a shrinking core and suggesting phase boundary motion perpendicular to the lithium flux, which could not be described by standard electrochemical kinetics. G. Ceder suggested adapting the Cahn-Hilliard (CH) model for bulk phase separation [41], but it took several years to achieve a consistent theory. Our initial model predicted intercalation waves [18, 32, 33], but did not uphold the De Donder relation [36], as became clear from discussions with K. Sekimoto and D. Lacoste at ESPCI in Paris. It was there during a sabbatical leave in 2007 that I first succeeded at generalizing BV kinetics to concentrated solutions. I spent the next year developing dynamical models of concentrated solutions [35], initially motivated by induced-charge electrokinetics [42]. By spring 2009, I synthesized the theory in lecture notes [31] and published the BV equation for concentrated solutions [35] (Sec. 5.4.2). (See also Sekimoto [36].)

The theory has enabled breakthroughs in modeling phase-separating battery electrodes. D. Burch used a thermodynamically consistent "Cahn-Hilliard-Reaction" model to study intercalation in nanoparticles [13] (with $\alpha = 0$), without connections to the battery voltage. His Ph.D. thesis [29] included early simulations of multi-particle phase separation and "mosaic instability" [27, 28]. Simulations of galvanostatic discharge by P. Bai and D. A. Cogswell led to a theory of the suppression of phase separation in nanoparticles [15], first reported in 2010 [34], which Cogswell [14] and Stanton [23] extended for coherency strain. Meanwhile, T. R. Ferguson did the first simulations of phase separation in porous electrodes [30].

We proceed to summarize the theory and some key predictions. First, a thermodynamic framework for reaction kinetics is applied to Faradaic reactions, thereby generalizing the Butler-Volmer and Marcus models to concentrated solutions and solids. The theory is then unified with phase-field models by formulating electrode kinetics in terms of thermodynamic variational principles. Finally, the theory is applied to intercalation dynamics in LFP nanoparticles.

II. BUTLER-VOLMER KINETICS IN CONCENTRATED SOLUTIONS

The theory begins with the diffusional chemical potential of species i,

$$\mu_i = k_B T \ln c_i + \mu_i^{ex} = k_B T \ln a_i \tag{3}$$

where c_i is the concentration, a_i is the absolute chemical activity, $\mu_i^{ex} = k_B T \ln \gamma_i$ is the excess chemical potential in a concentrated solution, and γ_i is the activity coefficient ($a_i = \gamma_i c_i$). In linear irreversible thermodynamics (LIT) [38, 39], the flux of species i is proportional to its chemical potential gradient,

$$F_i = -M_i c_i \nabla \mu_i = -D_i \left(\nabla c_i + c_i \nabla \frac{\mu_i^{ex}}{k_B T} \right) = -D_i^{chem} \nabla c_i \tag{4}$$

where D_i is the tracer diffusivity, $M_i = D_i / k_B T$ is the mobility (using the Einstein relation), and $-\nabla \mu_i^{ex}$ is the thermodynamic driving force beyond ideal diffusion (first term). By including the mean electrostatic energy ($z_i e \phi$ below) in the *electro*-chemical potential, this approach has been widely used to describe concentrated solutions in electrochemical systems [2] and electrokinetic phenomena [35].

The total flux in Eq. 4 has two contributions: (i) free diffusion driven by concentration gradients (Fick's law), and (ii) migration induced by gradients in *excess* chemical potential. In a thermodynamically consistent formulation of reaction kinetics [31, 36], therefore, the reaction complex explores a landscape of *excess* chemical potential $\mu^{ex}(x)$ between local minima μ_1^{ex} and μ_2^{ex} with transitions over an activation barrier $\mu_\ddagger^{ex}$. For the general chemical reaction, $S_1 = \sum_i s_i M_i \rightarrow \sum_j s_j M_j = S_2$, the activities, $a_1 = \prod_i a_i^{s_i}$ and $a_2 = \prod_j a_j^{s_j}$, are equal in equilibrium, and the forward and backward reactions obey detailed balance ($R = 0$). Out of equilibrium, assuming long-lived states with rare transitions ($\mu_\ddagger^{ex} - \mu_i^{ex} \gg k_B T$), the net reaction rate is given by

$$\begin{aligned} R &= R_{1\rightarrow 2} - R_{2\rightarrow 1} \\ &= \nu \left[c_1 e^{-(\mu_\ddagger^{ex} - \mu_1^{ex})/k_B T} - c_2 e^{-(\mu_\ddagger^{ex} - \mu_2^{ex})/k_B T} \right] \\ &= \nu \left[e^{-(\mu_\ddagger^{ex} - \mu_1)/k_B T} - e^{-(\mu_\ddagger^{ex} - \mu_2)/k_B T} \right] \\ &= \frac{\nu(a_1 - a_2)}{\gamma_\ddagger} \end{aligned} \tag{5}$$

which automatically satisfies the De Donder relation [36], $\mu_1 - \mu_2 = k_B T \ln(R_{1\to 2}/R_{2\to 1})$. Extending Kramer's escape formula [37], the frequency prefactor ν depends on generalized force constants, $k_i = \frac{\partial^2 \mu^{ex}}{\partial x_i^2}$, at the saddle point and in one minimum (e.g. state 1, with a suitable shift of $\mu_\ddagger^{ex}$).

For the general electrode reaction,

$$S_1 = O^{z_O} + ne^- \to R^{z_R} = S_2 \tag{6}$$

we write $\mu_1 = \mu_O + n\mu_e$ and $\mu_2 = \mu_R$, where charge conservation implies $z_O - n = z_R$. We decompose the *electro*-chemical potential into chemical and electrostatic contributions,

$$\mu_i = k_B T \ln a_i + z_i e\phi_i = (k_B T \ln c_i + z_i e\phi_i) + \mu_i^{ex} \tag{7}$$

where the term in parentheses describes an ion of charge $z_i e$ in a mean potential ϕ_i in a dilute solution, and $\mu_i^{ex} = k_B T \ln \gamma_i$ is the excess chemical potential. The electrostatic potential of electrons in the electrode is ϕ_e, while that of the electrolytic solution is ϕ. The difference is the interfacial voltage, $\Delta\phi = \phi_e - \phi$.

Let us consider the broad class of Faradaic reactions where the oxidized state is in the electrolyte (e.g .solvated Li^+), and the reduced state is either there, or inserted in the electrode as a neutral species (e.g. a Li^+/e^- polaron). The electrochemical potentials of the species in Eq. 6 are

$$\mu_O = k_B T \ln a_O + z_O e\phi \tag{8}$$
$$\mu_R = k_B T \ln a_R + z_R e\phi \tag{9}$$
$$\mu_e = k_B T \ln a_e - e\phi_e \tag{10}$$

where μ_e is the chemical potential of electrons, or Fermi level. The electron activity $a_e = \gamma_e c_e$ accounts for the concentration of free electrons c_e (density of states), as well as shifts in the Fermi level via γ_e, due to applied stress, phase transformations, donor or acceptor ions, etc. as illustrated below for semiconducting electrodes.

In equilibrium ($\mu_1 = \mu_2$), the interfacial voltage, $\Delta\phi = \phi_e - \phi$, satisfies the Nernst equation

$$\Delta\phi^{eq} = \frac{k_B T}{n_c e} \ln \frac{a_O a_e^n}{a_R} \tag{11}$$

where $n_c = n$. Out of equilibrium, the current $I = neAR$ (where A = electrode area) is related to the local (activation, or surface) over-potential,

$$\eta = \Delta\phi - \Delta\phi^{eq} \tag{12}$$

Specific models of charge transfer correspond to different choices of $\mu_\ddagger^{ex}$.

In order to generalize Butler-Volmer kinetics, we approximate the mean electrostatic energy of the transition state as a linear combination of those of the initial and final states:

$$\mu_\ddagger^{ex} = k_B T \ln \gamma_\ddagger + \alpha_a (z_O e\phi - ne\phi_e) + \alpha_c z_R e\phi \tag{13}$$

If, for consistency, the electric field is constant across the reaction coordinate x from x_R to x_O past the transition state at $x_R < x_\ddagger < x_O$, then the transfer coefficients, $\alpha_a = 1 - \alpha$ and $\alpha_c = \alpha$, are related to the symmetry factor,

$$\alpha = \frac{x_\ddagger - x_R}{x_O - x_R} = \alpha_c = 1 - \alpha_a, \tag{14}$$

which acts as a Brønsted coefficient [3].

Substituting Eq. 11-Eq. 14 into Eq. 5, we obtain the BV equation Eq. 1 with

$$I_0 = \nu neA (c_O c_e^n)^{1-\alpha} c_R^\alpha \left\{ \frac{(\gamma_O \gamma_e^n)^{1-\alpha} \gamma_R^\alpha}{\gamma_\ddagger} \right\} \tag{15}$$

The first factor is the classical formula [1, 2], but this is only valid for dilute solutions ($\gamma_O = \gamma_R = \gamma_\ddagger = \gamma_e = 1$). The second factor in braces modifies the exchange current for concentrated solutions. In summary, the Faradaic current I is related to the interfacial voltage $\Delta\phi$ and the various chemical activities a_O, a_R, a_e, and $\gamma_\ddagger$ by Eq. 1, Eq. 11, Eq. 12, and Eq. 15.

III. MARCUS THEORY FOR CONCENTRATED SOLUTIONS

Just as we have reformulated Butler-Volmer kinetics for concentrated solutions, so it is also possible to adapt the microscopic theory of charge transfer. The basic idea (1) is that the Faradaic reaction Eq. 6 occurs when the *excess* chemical potential of the reduced state, deformed along the reaction coordinate by statistical fluctuations, equals that of the oxidized state (plus n electrons in the electrode) at the same point. More precisely, charge transfer occurs randomly at somewhat lower energies due to quantum tunneling [1, 3].

As a first approximation [1, 3], we postulate harmonic restoring potentials for structural relaxation (e.g. shedding of the solvation shell from a liquid, or extraction from a solid) along the reaction coordinate x from the oxidized state at x_O to the reduced state at x_R:

$$\mu_1^{ex}(x) = k_B T \ln(\gamma_O \gamma_e^n) + z_O e\phi - ne\phi_e + \frac{k_O}{2}(x - x_O)^2 \tag{16}$$

$$\mu_2^{ex}(x) = k_B T \ln \gamma_R + z_R e\phi + \frac{k_R}{2}(x - x_R)^2 \tag{17}$$

The Nernst equation Eq. 11 follows by equating the *total* chemical potentials at the local minima, $\mu_1(x_O) = \mu_2(x_R)$ in equilibrium. The free energy barrier is set by the intersection of the *excess* chemical potential curves for the initial and final states, $\mu_\ddagger^{ex} = \mu_1^{ex}(x_\ddagger) = \mu_2^{ex}(x_\ddagger)$, which is an implicit equation for the barrier position, $x = x_\ddagger$. Using Eq. 11 and Eq. 12, we obtain

$$ne\eta - k_B T \ln \frac{c_R}{c_O c_e^n} = \frac{k_O}{2}(x_\ddagger - x_O)^2 - \frac{k_R}{2}(x_\ddagger - x_R)^2 = \mu_2^{ex}(x_R) - \mu_1^{ex}(x_O) = \Delta G^{ex} \tag{18}$$

where ΔG^{ex} is the *excess* free energy change per reaction.

The overpotential is the *total* free energy change per charge transferred,

$$ne\eta = ne\Delta\phi - k_BT \ln \frac{a_O a_e^n}{a_R} = \mu_2(x_O) - \mu_1(x_R) \quad (19)$$

and

$$\Delta G = ne\eta = \Delta G^{ex} + k_BT \ln \frac{c_R}{c_O c_e^n} \quad (20)$$

is the thermodynamic driving force for the reaction. In classical Marcus theory [1, 4], the overpotential is defined by $ne\eta = \Delta G^{ex}$ without the concentration factors required by non-equilibrium thermodynamics, which is valid for charge-transfer reactions in bulk phases ($A^- + B \rightarrow A + B^-$) because the initial and final concentrations are the same, and thus $\Delta G = \Delta G^{ex} = \Delta G^0$ (standard free energy of reaction). For Faradaic reactions at interfaces, however, the concentrations of reactions and products are different, and Eq. 20 must be used. The missing "Nernst concentration term" in Eq. 20 has also been noted by Kuznetsov and Ulstrup [3] (p. 219).

Following Marcus, we solve Eq. 18 for $x_\ddagger$ and relate $\mu_\ddagger^{ex}$ to η. For symmetric relaxation, $k_O = k_R = k$, we obtain the barriers for the cathodic and anodic reactions,

$$\Delta G_c^{ex} = \mu_\ddagger^{ex} - \mu_1^{ex}(x_O) = \frac{\lambda}{4}\left(1 + \frac{\Delta G^{ex}}{\lambda}\right)^2 \quad (21)$$

$$\Delta G_a^{ex} = \mu_\ddagger^{ex} - \mu_2^{ex}(x_R) = \frac{\lambda}{4}\left(1 - \frac{\Delta G^{ex}}{\lambda}\right)^2 \quad (22)$$

respectively, in terms of the reorganization energy, $\lambda = \frac{k}{2}(x_O - x_R)^2$.

Substituting $\mu_\ddagger^{ex}$ into Eq. 5, the current $I = neAR$ is given by

$$I = I_0 e^{(ne\eta)^2/4k_BT\lambda}\left(e^{-\alpha ne\eta/k_BT} - e^{(1-\alpha)ne\eta/k_BT}\right) \quad (23)$$

which has a stronger nonlinear dependence on overpotential than in the Butler-Volmer equation. The exchange current,

$$I_0 = neAe^{-\lambda/4k_BT}(c_O c_e^n)^{1-\alpha} c_R^\alpha, \quad (24)$$

and symmetry factor,

$$\alpha = \frac{1}{2}\left(1 - \frac{k_BT}{\lambda}\right) \quad (25)$$

are both related to the reorganization energy λ. In the typical case, $\lambda \gg k_BT$ (for thermally stable solvation), the symmetric factor is $\alpha \approx \frac{1}{2}$, and the current Eq. 23 is well approximated by the Butler-Volmer equation up to fairly large overpotentials, $|\eta| \ll \frac{k_BT}{ne}\sqrt{\frac{\lambda}{k_BT}}$. Comparing Eq. 24 with Eq. 15, we can relate the reorganization energy to the activity coefficients defined above,

$$\frac{\lambda}{4} = k_BT \ln \frac{\gamma_\ddagger}{(\gamma_O \gamma_e^n)^{1-\alpha}\gamma_R^\alpha} = (1-\alpha)\Delta G_c^{ex} + \alpha \Delta G_a^{ex} \quad (26)$$

which is an average barrier for the cathodic and anodic reactions, weighted by the symmetry factor.

In a dilute solution, the reorganization energy λ_0 can be estimated by the classical Marcus approximation, $\lambda_0 = \lambda_i + \lambda_o$, where is the "inner" or short-range contribution from structural relaxation (sum over normal modes) and λ_o is the "outer", long-range contribution from the Born energy of solvent dielectric relaxation [1, 4]. For polar solvents at room temperature, the large Born energy, $\lambda_o > 0.5n^2\text{eV} \approx 20n^2k_BT$, implies that single-electron ($n = 1$), symmetric ($\alpha \approx \frac{1}{2}$) charge transfer is favored. Many quantum mechanical expressions for λ_0 are also available [3].

In a concentrated solution, we can use various models below to estimate the thermodynamic correction, $\gamma_\ddagger^c$, due to entropic and enthalpic effects in the transition state. The exchange current can then be modeled by Eq. 15 with

$$\gamma_\ddagger = \gamma_\ddagger^c e^{\lambda_0/4k_BT}. \quad (27)$$

where α given by Eq. 25 with $\lambda = \lambda_0$. For example in surface adsorption, if the transition state excludes s sites, $\gamma_\ddagger^c = (1-c)^{-s}$, then Eq. 27 reduces to

$$\gamma_\ddagger = \frac{e^{E_\ddagger/k_BT}}{(1-c)^s} \quad (28)$$

where $E_\ddagger = \frac{\lambda_0}{4}$, consistent with Eq. 26. This approach provides a thermodynamically consistent way to model the combined effects of solvation, structural relaxation, enthalpy and entropy on charge transfer kinetics in a concentrated solution, ionic liquid or solid.

IV. ION INTERCALATION KINETICS

Let us apply the general theory above to lithium insertion in a homogeneous solid solution, $Li^+ + e^- \rightarrow Li_{(s)}$. (See Eq. 43 below for extensions to heterogeneous solid solutions with mechanical deformation.) Although lithium ions may remain charged, they typically exist as neutral quasiparticles (Li^+M^- polarons [3]) coupled to electrons localized on solid atoms (M). For example, the standard model for $LiFePO_4$ [13–15, 18, 41] is a regular solution [39, 43] for the reduced state R =Li with mole fraction c,

$$\mu_{Li} = k_BT \ln \frac{c}{1-c} + \Omega(1-2c) \quad (29)$$

where the first term is the configurational entropy and the second the enthalpy of mixing (setting $\mu = 0$ at half filling as a reference). The Nernst potential (Eq. 11) is

$$\Delta\phi(c) = \Delta\phi^0 - \frac{\mu_{Li}(c)}{e} + \frac{k_BT}{e}\ln a_e(c) \quad (30)$$

and, for insertion at the cathode, the open circuit voltage of the battery is $V_O(c) = \Delta\phi(c) - \Delta\phi_{anode}$. If the

transition state excludes s sites (where $s > 1$ accounts for the Li^+ solvation shell) and has reorganization energy λ_0, then using Eq. 28 the exchange current Eq. 15 takes the form,

$$I_0(c) = eA(a_+ a_e(c))^{1-\alpha} c^\alpha (1-c)^{s-\alpha} \exp\left(\frac{4\alpha\Omega(1-2c) - \lambda_0}{4k_BT}\right) \tag{31}$$

where a_+ is the Li^+ activity in the electrolyte and $a_e(c)$ is the electron activity, which can depend on c, e.g. if Li acts as a donor impurity in a semiconducting insertion electrode.

This example illustrates how the theory unifies charge-transfer kinetics with battery thermodynamics. In porous electrode models for Li-ion batteries [2, 5, 7], the rate expression Eq. 2 is assumed, which corresponds to Eq. 31 with $a_+ = a_e = 1$, $\Omega = 0$, and $s = 1$. The dilute electrolyte activity, $a_+ = c_+$ has also been included [7], but these models are inconsistent with the use of concentrated solution models ($a_+ \neq c_+$) to fit experimental data. A more serious inconsistency is the fitting of the open circuit voltage, $V_O(c)$, which should be related to the local ionic activities Eq. 29 in both the Nernst equation, Eq. 30, and the exchange current density, Eq. 31. It is also inconsistent to model solid diffusion by Fick's law with a fitted nonlinear diffusivity, rather than using ionic activity gradients in Eq. 4.

V. VARIATIONAL FORMULATION OF ELECTRODE KINETICS

In order to describe phase separation, we adopt the Cahn-Hilliard (CH) model, based on the Helmholtz free energy functional,

$$F[c] = \int_V \left[\rho_s \bar{f}(c) + \frac{1}{2}\nabla c \cdot \kappa \nabla c\right] dV \tag{32}$$

where κ is the "gradient penalty tensor" [39, 43]. (We define $\bar{f}$ and c per crystal site, and introduce the site density ρ_s.) The bulk chemical potential is defined variationally,

$$\mu = \frac{1}{\rho_s}\frac{\delta F}{\delta c} = \bar{f}'(c) - \frac{\nabla \cdot \kappa \nabla c}{\rho_s} \tag{33}$$

as the free-energy change for adding a bulk "particle" (delta function δc). If $\bar{f}(c)$ has multiple minima representing distinct stable phases, then the gradient term counteracts the tendency to phase separate and leads to a diffuse interface, whose equilibrium profile satisfies $\mu =$ constant.

There were several breakthroughs in 2004 that set the stage for our work. Han et al. [41] first applied the CH equation to model diffusion in LFP using the regular solution model (Eq. 29). Garcia et al. [44] formulated variational principles for electromagnetically active systems, which unify the CH equation with Maxwell's equations. Guyer et al. [45] first represented a diffuse electrode/electrolyte interface with a continuous phase field. They described the kinetics of electrodeposition [46] by linear Allen-Cahn kinetics [39], $I \propto \Delta\mu$, but did not make connections with charge-transfer theory.

Our theory followed from these developments and the observation of phase boundaries at LFP surfaces [40, 47]. The exponential (Tafel) dependence of the current on the overpotential, defined in terms of $\Delta\mu$ in Eq. 33, was first reported in 2007 [18, 32, 33], but with a spurious prefactor, noted by Burch [13, 29]. The complete theory, connecting the CH model to the BV equation and the battery voltage, appeared in 2009 [31] and was later applied to LFP nanoparticles [14, 15]. For lithium intercalation, the reduced state has zero charge ($z_R = 0$), so the original CH functional Eq. 32 with $\bar{f}(c)$ given by Eq. 29 was used to construct the electrochemical potential Eq. 33 in the Butler-Volmer and Nernst equations.

For the general Faradaic reaction,

$$O + ne^- = \sum_i s_i O_i^{z_i} + ne^- \rightarrow \sum_j s_j R_j^{z_j} = R, \tag{34}$$

we define all the chemical activities a_k and diffusional electrochemical potentials μ_k variationally from the Gibbs free energy G:

$$\mu_O = k_BT \ln a_O + z_O e\phi_O = \sum_i \frac{s_i}{\rho_s}\frac{\delta G}{\delta c_i} \tag{35}$$

$$\mu_R = k_BT \ln a_R + z_R e\phi_R = \sum_j \frac{s_j}{\rho_s}\frac{\delta G}{\delta c_j} \tag{36}$$

$$\mu_e = k_BT \ln a_e - e\phi_e = \frac{1}{\rho_s}\frac{\delta G}{\delta c_e} \tag{37}$$

The Nernst voltage $\Delta\phi^{eq}$ is defined variationally by setting $\mu_R = \mu_O + n\mu_e$. According to Eq. 11, Eq. 12 and Eq. 20, the activation overpotential

$$\eta = \frac{\mu_R - (\mu_O + n\mu_e)}{ne} = \frac{\mu_2 - \mu_1}{ne} \tag{38}$$

is the change in *total* chemical potential of the Faradaic reaction per charge transferred ($n_c = n$). In this way, the diffusional electrochemical potentials $\mu_i = \frac{\delta G}{\rho_s \delta c_i}$ enter the Butler-Volmer (Eq. 1) and Marcus (Eq. 23) equations, as well as the exchange current Eq. 15.

The following free energy captures the key physics of ionic materials [13–15, 18, 44, 45, 48]:

$$\begin{aligned} G = \int_V \Big[&\rho_s\left(\bar{f}(\vec{c}) + \rho_e\phi\right) \\ &+\frac{1}{2}\left(\nabla\vec{c}\cdot\kappa\nabla\vec{c} - \nabla\phi\cdot\varepsilon_p\nabla\phi + \sigma:\epsilon\right)\Big] dV \\ &+ \oint_S \gamma_s(\hat{n},\vec{c},\phi) dS \end{aligned} \tag{39}$$

where $\vec{c}$ is the set of concentrations, ε_p the permittivity tensor, κ the gradient penalty tensor, σ the stress tensor, ϵ the strain tensor, γ_s the surface tension, and $\rho_e = \sum_i z_i e c_i$ the bulk charge density. The electrostatic

potential acts as a Lagrange multiplier controlling the total ion densities [14, 44] while enforcing Maxwell's equations [48]. Assuming linear elasticity, the stress is given by Hooke's law, $\sigma_{ij} = C_{ijkl}\epsilon_{kl}$, where C is the elastic constant tensor. The lattice-preserving "coherency strain",

$$\epsilon_{ij} = \frac{1}{2}\left(\frac{\partial u_i}{\partial x_j} + \frac{\partial u_j}{\partial x_i}\right) - \sum_m \epsilon^0_{ijm} c_m \tag{40}$$

is the total strain due to compositional inhomogeneity (first term) relative to the stress-free inelastic strain (second term). In a mean-field approximation (Vegard's law), each molecule of species m exerts an independent strain ϵ^0_m (lattice misfit between $c_m = 0, 1$).

Through the electro-chemical potentials,

$$\begin{aligned}\mu_i &= \left(\frac{\partial \bar{f}}{\partial c_i} - \frac{\nabla\cdot\kappa\nabla c_i + \sigma : \epsilon^0_i}{\rho_s}\right) + z_i e\phi \\ &= k_B T \ln a_i + z_i e\phi\end{aligned} \tag{41}$$

the Nernst voltage Eq. 11 and exchange current Eq. 15 have novel dependencies on concentration gradients and elastic stress, which lead new modes of ion intercalation (2). For ion insertion (1), we can model the transition state as

$$\gamma_\ddagger = (1-c_i)^{-s} \exp\left[\frac{1}{k_B T}\left(\frac{\lambda_0}{4} - \frac{\sigma : \epsilon_\ddagger}{\rho_s}\right)\right] \tag{42}$$

where $\epsilon_\ddagger$ is the transition-state strain, $s \geq 1$ the number of excluded sites, and λ_0 the reorganization energy. For insertion in a regular solid solution, the exchange current is

$$I_0 = \bar{I}_0(c) \exp\left(\frac{\sigma : \Delta\varepsilon - \alpha(\nabla\cdot\kappa\nabla c)}{\rho_s k_B T}\right) \tag{43}$$

where $\bar{I}_0(c)$ is the limit of zero stress and uniform concentration Eq. 31 and $\Delta\varepsilon = \epsilon_\ddagger - \alpha\epsilon^0$, is the "activation strain" [49].

From the LIT flux Eq. 4, conservation of mass leads to the CH equation,

$$\frac{\partial c_i}{\partial t} + \nabla\cdot\mathbf{F}_i = \bar{R}_i, \quad \text{where} \quad \mathbf{F}_i = -\frac{D_i c_i}{k_B T \rho_s}\nabla\frac{\delta G}{\delta c_i}. \tag{44}$$

The homogeneous reaction rate $\bar{R}_i$, describing bulk charge transfer reactions (e.g. water self-ionization), is often neglected, but could be described by our theory. The current density is also expressed variationally, $\mathbf{J} = \sum_i z_i e \mathbf{F}_i$. The CH equation is fourth-order and requires two boundary conditions at each interface. One relates the normal flux to the reaction rate, $\hat{n}\cdot\mathbf{F}_i = R_i$, where $R_i = 0$ for an inactive species and $R_i = \frac{J}{s_i z_i e}$ for an active species. The other is the "variational boundary condition",

$$[\hat{n}\cdot\kappa\nabla c_i] = \frac{\partial \gamma_s}{\partial c_i} \tag{45}$$

(where [X] denotes the jump in X at an interface), which ensures continuity of the chemical potential [13] and controls surface wetting and nucleation [15].

VI. ION INTERCALATION WITH PHASE SEPARATION

Size-dependent solubility. It is well known that the spinodal gap of unstable compositions in a solid solution shrinks with decreasing particle size [50], as low energy long-wavelength fluctuations are prohibited. The miscibility gap also shrinks, since the relative cost of a phase boundary increases with the surface to volume ratio [51]. Elastic coherency strain enhances both effects by increasing the energy penalty for phase separation [12, 14, 21].

The theory predicts novel effects of *kinetics* on solubility, due to ion exchange with the electrolyte reservoir [13, 14]. At constant voltage, the spinodal and miscibility gaps shrink with increasing exchange current [13], since fluctuations with fast reactions promote unfavorable concentration gradients. Experimental solubility data [17] can be interpreted using a 1D Cahn-Hilliard-reaction (CHR) model [13, 29], or a more accurate, 2D reaction-limited model with coherency strain [14].

Intercalation waves. In anisotropic crystals, ion intercalation dynamics can be limited by diffusion or reactions, independently in each direction [18]. In LFP nanoparticles, the concentration tends to remain uniform in the [010] direction due to the fast diffusion [19, 52] and elastically unfavorable phase separation [14] in short one-dimensional channels, unblocked by Fe anti-site defects [20]. After [010] depth-averaging [18], the full CHR model reduces to a new, reaction-limited model on the active {010} crystal facet,

$$\frac{\partial c}{\partial t} = J_0\, f(\eta), \tag{46}$$

(where $J_0 = I_0/A_s$ is the current per surface site), which is an electrochemical generalization of the Allen-Cahn equation [39] (EAC) with with a nonlinear dependence on the variational overpotential,

$$\eta = \frac{1}{e\rho_s}\frac{\delta G}{\delta c} + \Delta\phi, \tag{47}$$

where $f(\eta) = I/I_0$ can come from the BV (Eq. 1) or Marcus (Eq. 23) equations. For lithium insertion in a regular solution [14, 15], the exchange current $I_0(c, \nabla\cdot\kappa\nabla c, \sigma)$ is given by Eq. 43.

The theory has led to a paradigm shift in understanding insertion dynamics. In contrast to prior battery models, which assume a uniform reaction rate over the particle surface, limited by radial solid diffusion [2, 5] or a shrinking-core phase boundary [6, 7], the EAC limit of the CHR model predicts reaction-limited intercalation waves (or "domino cascades" [53]), sweeping across the active facet, filling the crystal layer by layer (2) [14, 15, 18, 33, 54]. Intercalation waves result from nucleation at surfaces or defects, or by spinodal decomposition [15], and trace out the voltage plateau at low current, as shown in 3. Experimental evidence of one-

dimensional nucleation and growth, consistent with the EAC theory [15, 18], has recently been reported [26].

Driven phase separation. The theory has led to some surprising conclusions about electrochemically driven phase transformations in nanoparticles. Our first paper included a proof that traveling-wave solutions of the EAC equation only exist over a finite range of thermodynamic driven force [18, 32], but the implications were unclear without the connection to the battery voltage. Once the generalization of BV kinetics was achieved [31], simulations and analysis revealed how phase separation is strongly influenced by the applied current [14, 15]. As suggested by Malik et al. [16] based on bulk free energy calculations, phase separation is suppressed during battery operation, but the mechanism is related to activation overpotential at the surface.

As explained by Bai et al. [15], phase separation is suppressed as the applied current approaches the exchange current. A linear stability analysis of the EAC model for BV kinetics with $\alpha = \frac{1}{2}$ shows that concentration fluctuations of wavenumber k grow at a rate [15]

$$s(k;c,I) = -\sqrt{\bar{J}_0 + \frac{I^2}{4}}(\bar{\eta}' + \kappa k^2) + I\left(\frac{\bar{J}_0'}{\bar{J}_0} + \frac{1}{2}\kappa k^2\right) \tag{48}$$

where $\bar{\eta}(c)$ and $\bar{J}_0(c)$ are the activation overpotential and exchange current density, respectively, in a homogeneous state of concentration c sustaining a current I. The range of linear instability, $s(c, I) > 0$, predicted by Eq. 48 and Eq. 43 with elastic strain is shown in 3(a).

The theory predicts a *critical current*, of order the exchange current, above which phase separation by spinodal decomposition is impossible. Below this current, the homogeneous state is unstable over a range of concentrations (smaller than the zero-current spinodal gap), but for large currents, the time spent in this region is too small for complete phase separation. Instead, the particle passes through a transient *quasi-solid solution* state, where its voltage and concentration profile resemble those of a homogeneous solid solution.

The suppression of phase separation predicted by the theory is very general. When nucleation is possible (see below), a similar current dependence is observed. As shown in 3, the bulk crystal fills ahead of the surface-nucleated intercalation waves in the quasi-solid solution regime, while homogeneous filling occurs above the critical current. With elastic coherency strain included, the suppression of phase separation is analogous, but even stronger [14].

In the case of LFP, the critical current is an order of magnitude smaller than the exchange current [14]. The surprising implication is that phase separation does not occur *in situ* during normal battery operation, which helps to explain the high-rate capability and extended lifetime of LFP nanoparticles, due to larger active area and smaller elastic stresses. On the other hand, phase separation occurs at very low currents and can be observed in particles trapped at intermediate compositions for *ex situ* measurements (4).

Phase separation patterns. For quantitative interpretation of experiments [14], it is essential to account for the elastic energy. Even a simple elastic model can dramatically improve the inference of lithium diffusivity from intermitted titration with phase separation [56]. Crystal anisotropy generally leads to striped patterns in equilibrium [21–23]. The stripe spacing follows from the balance between elastic energy (favoring short wavelengths at a stress-free boundary) and interfacial energy, favoring long wavelengths to minimize interfacial area [14]. In layered crystals, the lattice misfit can cause tension and compression in different directions, and Stanton and Bazant [23] predicted that this could cause phase boundaries to tilt with respect to the crystal axes. For example, lithium insertion in LFP causes contraction of the iron phosphate planes in the [001] direction and expansion in the [100] and [010] directions [40]. Cogswell and Bazant [14] explained the experimentally observed phase morphologies [47, 55] and used the theory to infer the gradient penalty κ from the stripe spacing. As shown in Fig. 4, the model enables realistic simulations of reaction-limited phase separation.

Surface wetting and nucleation. The theory also predicts how surface thermodynamics affects reaction kinetics. Using the boundary condition Eq. 45 for the EAC equation Eq. 46, the nucleation of intercalation waves in LFP nanoparticles due to wetting of the {100} facet can be simulated with (2b) or without (3c) coherency strain [15]. The nucleation barrier (critical voltage past the equilibrium plateau to observe a sudden current) can be predicted as a function of particle size, in excellent agreement with experiments (D. A. Cogswell, unpublished). The effect of surface wetting on intercalation kinetics may be responsible for the surprising performance boost from phosphate-glass thin films on active nanoparticles of LFP [10] and Li_xCoO_2 [57].

Mosaic Instability. The complex dynamics of ion intercalation in nanoparticles also affects the macrosopic response of a composite electrode. Using the CHR model [13] for a collection of particles in a reservoir of constant chemical potential, Burch [29] discovered what we called the mosaic instability, whereby particles filling uniformly at constant total current suddenly fill one-by-one. The mechanism is simple: As the particles enter the miscibility gap, the first to phase separate will suddenly lower its chemical potential and sustain a much larger current until it becomes full, at which point the current is shared by the others until the process repeats. Interestingly, in the CHR model, the smaller particles transform first, because diffusion brings the core concentration to the spinodal more quickly. In contrast, for reaction-limited particles, the larger ones are more likely to nucleate first.

Meanwhile, Dreyer et al. [27] described the mosaic instability and demonstrated it experimentally in two clever ways. They connected it to the zero-current voltage gap between charge/discharge cycles in LFP batter-

ies, as well as the dynamics of an array of balloons connected to a single pressure line. Their theory [27, 28] is similar to the "pseudo capacitor limit" of our models, where each particle maintains uniform (but time dependent) concentration, without internal phase separation.

Porous electrodes. The theory has recently been extended to porous electrodes undergoing phase transformations [30] using classical porous electrode models to describe the electrolyte [2]. Diffusion in the electrolyte provides a spatiotemporal bias for the mosaic instability, so that narrow fronts of stochastic particle phase transformations propagate away from the separator (discharge) or current collector (charge) at low current (5). The width of the reaction front separating low-density and high-density phases increases with current until the entire electrode becomes active, which is a macroscopic analog of the suppression of phase separation in nanoparticles.

The theory can predict experimental data for phase-separating porous electrodes for the first time without artificially fitting voltage plateaus or enforcing phase boundaries. Using the EAC regular-solution model for LFP [14, 15] in a porous electrode [30], the model can predict tiny voltage oscillations ($< k_BT/e$ =25mV) and the limiting "voltage gap" at very low currents observed in experiments [27], which give way to a smoothly decaying voltage at high current [10] (5). Nucleation is also important at the porous electrode scale [26] and can be naturally included in theory. Using a two-component regular solution model for graphite intercalation [31], the theory is also able to fit experimental data for diffusion-limited intercalation of long graphite anodes [58] with multiple reaction fronts of different colors corresponding to different stages of lithiation.

VII. CONCLUSION

This Account describes the development of a theory of electrochemical kinetics in condensed matter. The theory has shed light on intercalation dynamics in advanced Li-ion batteries with phase-separating nanoparticles. Other possible applications include oxygen electrocatalysis in fuel cells and electrochemical stability of ionic liquids.

This work was supported by the National Science Foundation under Contracts DMS-0842504 and DMS-0948071 and by the MIT Energy Initiative.

BIOGRAPHICAL INFORMATION

Martin Z. Bazant received his B.S. (Physics, Mathematics, 1992) and M.S. (Applied Mathematics, 1993) from the University of Arizona and Ph.D. (Physics, 1997) from Harvard University. He joined the faculty at MIT in Mathematics in 1998 and Chemical Engineering in 2008. His honors include an Early Career Award from the Department of Energy (2003), Brilliant Ten from *Popular Science* (2007), and Paris Sciences Chair (2002,2007) and Joliot Chair (2008,2012) from ESPCI (Paris, France).

[1] A. J. Bard and L. R. Faulkner, *Electrochemical Methods* (J. Wiley & Sons, Inc., New York, NY, 2001).
[2] J. Newman, *Electrochemical Systems* (Prentice-Hall, Inc., Englewood Cliffs, NJ, 1991), 2nd ed.
[3] A. M. Kuznetsov and J. Ulstrup, *Electron Transfer in Chemistry and Biology: An Introduction to the Theory* (Wiley, 1999).
[4] R. A. Marcus, Rev. Mod. Phys. **65**, 599 (1993).
[5] M. Doyle, T. F. Fuller, and J. Newman, Journal of the Electrochemical Society **140**, 1526 (1993).
[6] V. Srinivasan and J. Newman, Journal of the Electrochemical Society **151**, A1517 (2004).
[7] S. Dargaville and T. Farrell, Journal of the Electrochemical Society **157**, A830 (2010).
[8] A. Padhi, K. Nanjundaswamy, and J. Goodenough, Journal of the Electrochemical Society **144**, 1188 (1997).
[9] J. Tarascon and M. Armand, Nature **414**, 359 (2001).
[10] B. Kang and G. Ceder, Nature **458**, 190 (2009).
[11] M. Tang, W. C. Carter, and Y.-M. Chiang, Annual Review of Materials Research **40**, 501 (2010).
[12] N. Meethong, H.-Y. S. Huang, W. C. Carter, and Y.-M. Chiang, Electrochem. Solid-State Lett. **10**, A134 (2007).
[13] D. Burch and M. Z. Bazant, Nano Letters **9**, 3795 (2009).
[14] D. A. Cogswell and M. Z. Bazant, ACS Nano **6**, 2215 (2012).
[15] P. Bai, D. Cogswell, and M. Z. Bazant, Nano Letters **11**, 4890 (2011).
[16] R. Malik, F. Zhou, and G. Ceder, Nature Materials **10**, 587 (2011).
[17] M. Wagemaker, D. P. Singh, W. J. Borghols, U. Lafont, L. Haverkate, V. K. Peterson, and F. M. Mulder, J. Am. Chem. Soc. **133**, 1022210228 (2011).
[18] G. Singh, D. Burch, and M. Z. Bazant, Electrochimica Acta **53**, 7599 (2008).
[19] D. Morgan, A. V. der Ven, and G. Ceder, Electrochemical and Solid State Letters **7**, A30 (2004).
[20] R. Malik, D. Burch, M. Bazant, and G. Ceder, Nano Letters **10**, 4123 (2010).
[21] N. Meethong, H. Y. S. Huang, S. A. Speakman, W. C. Carter, and Y. M. Chiang, Adv. Funct. Mater. **17**, 11151123 (2007).
[22] A. V. der Ven, K. Garikipati, S. Kim, and M. Wagemaker, J. Electrochem. Soc. **156**, A949A957 (2009).
[23] L. G. Stanton and M. Z. Bazant, submitted, arXiv:1202.1626v1 [cond-mat.mtrl-sci] (2011).
[24] A. V. der Ven and M. Wagemaker, Electrochemistry Communications **11**, 881884 (2009).
[25] M. Wagemaker, F. M. Mulder, and A. V. der Ven, Advanced Materials **21**, 27032709 (2009).
[26] G. Oyama, Y. Yamada, R. ichi Natsui, S. ichi Nishimura, and A. Yamada, J. Phys. Chem. C (2012).
[27] W. Dreyer, J. Jamnik, C. Guhlke, R. Huth, J. Moskon, and M. Gaberscek, Nat. Mater. **9**, 448 (2010).
[28] D. Dreyer, C. Guhlke, and R. Huth, Physica D **240**, 1008

(2011).
[29] D. Burch, *Intercalation Dynamics in Lithium-Ion Batteries* (Ph.D. Thesis in Mathematics, Massachusetts Institute of Technology, 2009).
[30] T. R. Ferguson and M. Z. Bazant (2012), submitted, arXiv:1204.2934v1 [physics.chem-ph].
[31] M. Z. Bazant, *10.626 Electrochemical Energy Systems* (Massachusetts Institute of Technology: MIT OpenCourseWare, http://ocw.mit.edu, License: Creative Commons BY-NC-SA, 2011).
[32] G. K. Singh, M. Z. Bazant, and G. Ceder (2007), arXiv:0707.1858v1 [cond-mat.mtrl-sci].
[33] D. Burch, G. Singh, G. Ceder, and M. Z. Bazant, Solid State Phenomena **139**, 95 (2008).
[34] P. Bai, D. A. Cogswell, and M. Z. Bazant, international Meeting on Lithium-Ion Batteries, Montreal, Canada, July, 2010.
[35] M. Z. Bazant, M. S. Kilic, B. Storey, and A. Ajdari, Advances in Colloid and Interface Science **152**, 48 (2009).
[36] K. Sekimoto, *Stochastic Energetics* (Springer, 2010).
[37] N. G. V. Kampen, *Stochastic Processes in Physics and Chemistry* (North-Holland, 2007), third edition.
[38] S. R. D. Groot and P. Mazur, *Non-equilibrium Thermodynamics* (Interscience Publishers, Inc., New York, NY, 1962).
[39] R. W. Balluffi, S. M. Allen, and W. C. Carter, *Kinetics of materials* (Wiley, 2005).
[40] G. Chen, X. Song, and T. Richardson, Electrochemical and Solid State Letters **9**, A295 (2006).
[41] B. Han, A. V. der Ven, D. Morgan, and G. Ceder, Electrochimica Acta **49**, 4691 (2004).
[42] M. Z. Bazant and T. M. Squires, Current Opinion in Colloid and Interface Science **15**, 203 (2010).
[43] J. W. Cahn and J. W. Hilliard, J. Chem Phys. **28**, 258 (1958).
[44] R. E. Garcia, C. M. Bishop, and W. C. Carter, Acta Mater. **52**, 11 (2004).
[45] J. E. Guyer, W. J. Boettinger, J. A. Warren, and G. B. McFadden, Phys. Rev. E **69**, 021603 (2004).
[46] J. E. Guyer, W. J. Boettinger, J. A. Warren, and G. B. McFadden, Phys. Rev. E **69**, 021604 (2004).
[47] L. Laffont, C. Delacourt, P. Gibot, M. Y. Wu, P. Kooyman, C. Masquelier, and J. M. Tarascon, Chem. Mater. **18**, 5520 (2006).
[48] M. Z. Bazant, B. D. Storey, and A. A. Kornyshev, Phys. Rev. Lett. **106**, 046102 (2011).
[49] M. J. Aziz, P. C. Sabin, and G. Q. Lu, Phys. Rev. B **41**, 9812 (1991).
[50] J. Cahn, Acta Metallurgica **9**, 795 (1961).
[51] E. B. Nauman and N. P. Balsara, Fluid Phase Equilib. **45**, 229250 (1989).
[52] M. S. Islam, D. J. Driscoll, C. A. J. Fisher, and P. R. Slater, Chem. Mater. **17**, 50855092 (2005).
[53] C. Delmas, M. Maccario, L. Croguennec, F. L. Cras, and F. Weill, Nature Materials **7**, 665 (2008).
[54] M. Tang, J. F. Belak, and M. R. Dorr, The Journal of Physical Chemistry C **115**, 4922 (2011).
[55] C. V. Ramana, A. Mauger, F. Gendron, C. M. Julien, and K. Zaghib, J. Power Sources **187**, 555564 (2009).
[56] Y. Zhu and C. Wang, Journal of Physical Chemistry C **114**, 2830 (2010).
[57] K. Sun and S. J. Dillon, Electrochemistry Communications **13**, 200 (2011).
[58] S. J. Harris, A. Timmons, D. R. Baker, and C. Monroe, Chemical Physics Letters **485**, 265274 (2010).

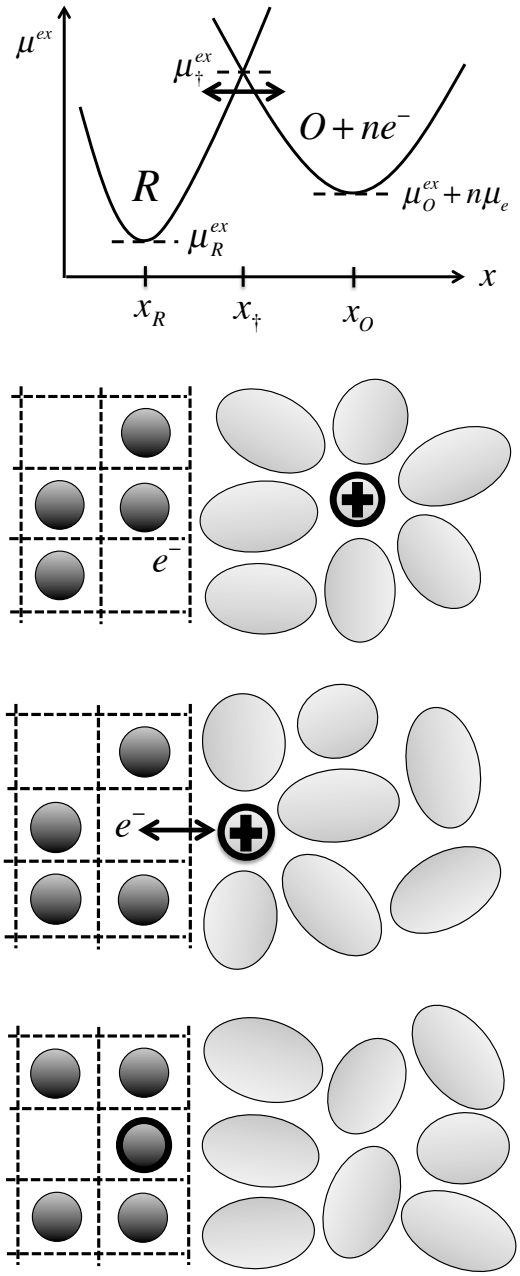

FIG. 1: Above: The Faradaic reaction $O + ne^- \rightarrow R$ in concentrated electrolyte and/or electrode solutions. The reactants fluctuate in a landscape of excess chemical potential μ^{ex}, shown along a favored reaction coordinate x. Charge transfer occurs whenever the oxidized state O with n free elections or the reduced state R reaches the transition state. Below: Illustration of these states for ion reduction by intercalation into a solid-solution electrode from a liquid electrolyte.

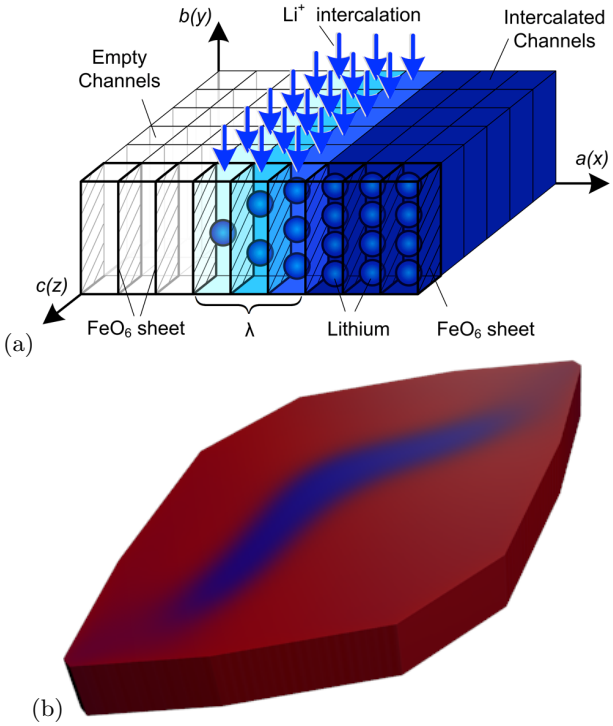

FIG. 2: Insertion kinetics in reaction-limited LFP nanoparticles. (a) The low-energy phase boundary between $FePO_4$ and $LiFePO_4$ propagates as an "intercalation wave" [11, 14, 15, 18, 33] across the {010} facet, filling the crystal layer by layer, as the reaction rate (Eq. 43) is enhanced by concentration gradients and elastic stress. [Bai et al. [15].] (b) Collision of intercalation waves nucleated by lithium wetting of the side facets prior to complete filling. [D. A. Cogswell, unpublished]

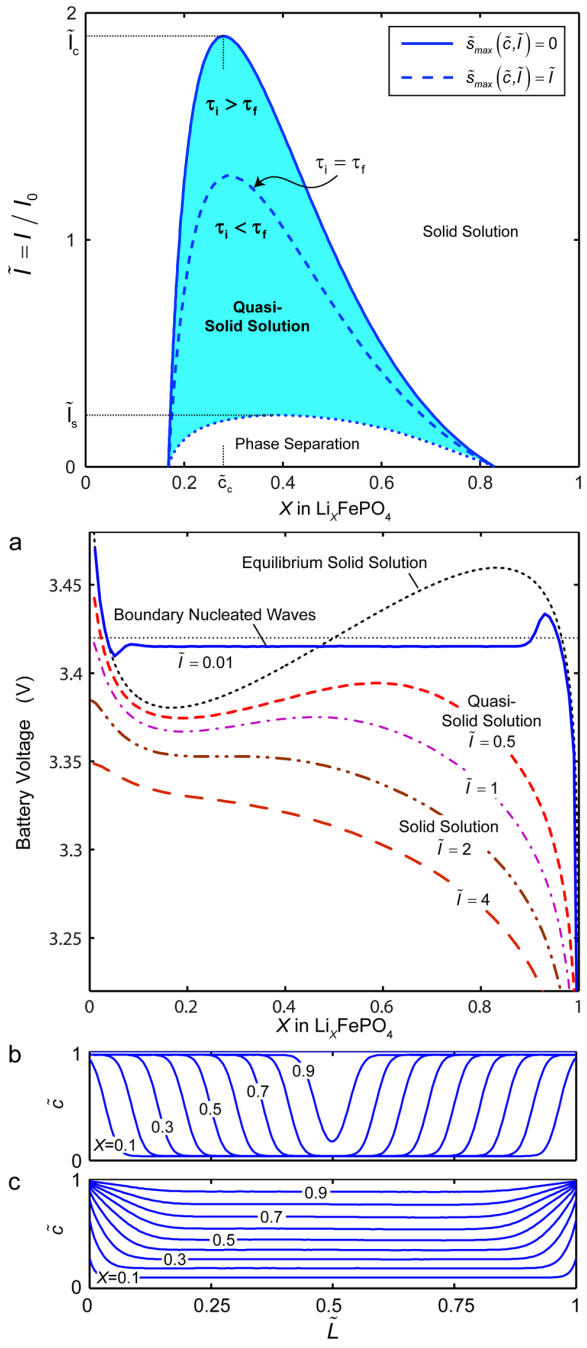

FIG. 3: Galvanostatic discharge into a single LFP cathode nanoparticle without coherency strain. Top: Linear stability (spinodal) diagram for the homogeneous state versus current $\tilde{I}$ (scaled to the exchange current at $X = 0.5$) and mean Li filling X. (a) Battery voltage versus state of charge (X) at different currents $\tilde{I}$. (b) Evolution of the concentration profile at low current $\tilde{I} = 0.01$ with insertion waves nucleated at the wetted [001] side facets. (c) Quasi-solid solution behavior close to the critical current $\tilde{I} = 0.5$, showing homogeneous filling ahead of the waves. [Bai et al. [15]]

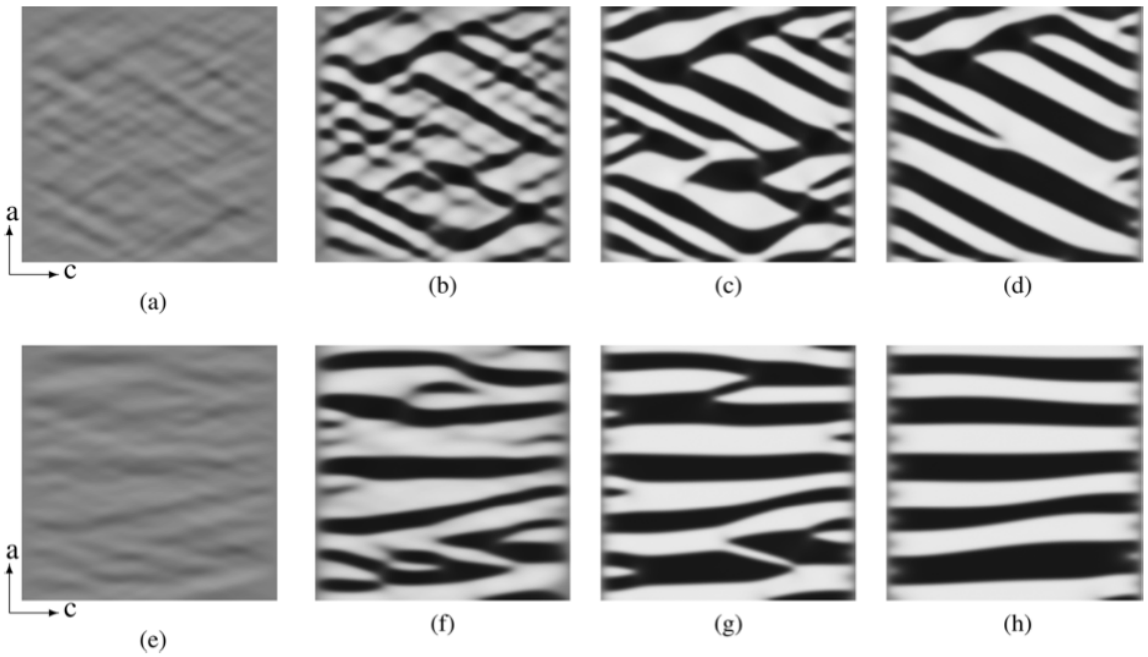

FIG. 4: Simulations of reaction-limited phase separation of a 500nm single crystal of $Li_{0.5}FePO_4$ into Li-rich (black) and Li-poor phases (white) in an electrolyte bath at zero current and zero pressure, consistent with *ex situ* experiments [40, 47, 55]. (a) Coherent phase separation, where lithium insertion causes contraction along [001] (c) axis and expansion along the [100] (a) axis, leading to tilted interfaces aligned with {101} planes. (b) Loss of [001] coherency (e.g. due to microcracks [40]) causes the phase boundaries to rotate to align with {100} planes. [Cogswell and Bazant [14].]

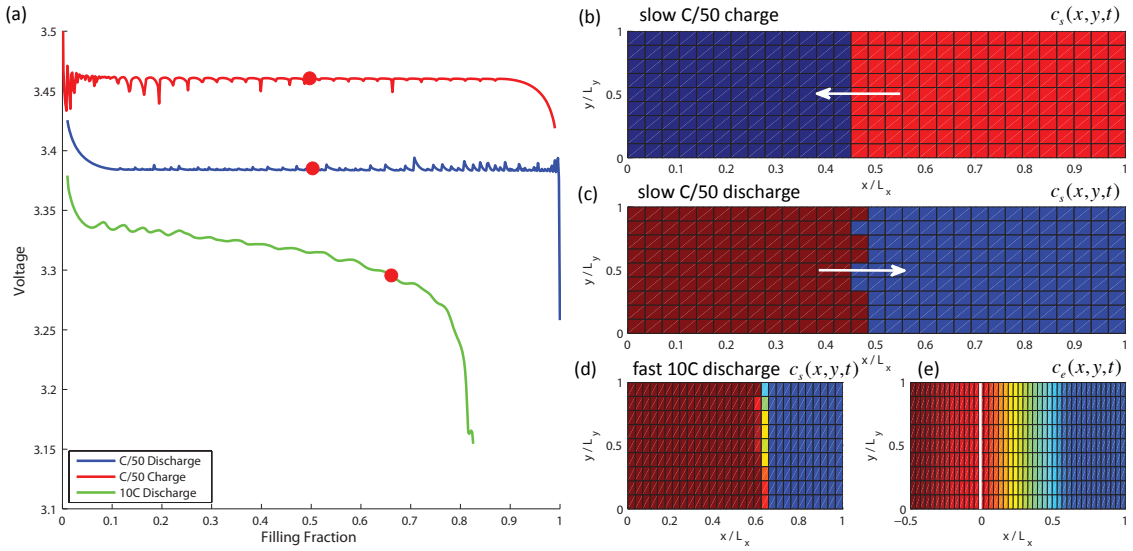

FIG. 5: Finite-volume simulations of macroscopic phase separation in a porous LFP cathode [30]. (a) Voltage versus state of charge for slow charge/discharge and fast discharge. (b)-(d) Profiles of mean Li concentration in the solid at the red points in (a), showing narrow reaction fronts with mosaic instabilities, associated with voltage fluctuations. (e) Electrolyte Li concentration for fast discharge (d), showing diffusion limitation. [Ferguson and Bazant [30]]